Global Optimization Study of Small ($10 \leq N \leq 120$) Pd Clusters Supported on MgO(100)

G. Rossi,[†] C. Mottet,[§] F. Nita,[†,‡] and R. Ferrando*[,†]

Dipartimento di Fisica, INFM and IMEM/CNR, Via Dodecaneso 33, Genova, I16146, Italy, Institute of Physical Chemistry "IG Murgulescu", Romanian Academy, Spl. Independentei 202, Bucharest, Romania, and CRMCN-CNRS, Campus de Luminy, case 913, 13288 Marseille Cedex 9, France

Received: November 15, 2005; In Final Form: February 17, 2006

Experimental evidence suggests that Pd clusters on MgO, known to be good reaction catalysts, have face centered cubic (fcc) epitaxial structures. The structure of such clusters is the result of the interplay of Pd−Pd and Pd−substrate bonds, the former inclined to favor icosahedral (Ih) and decahedral (Dh)-like structures, the latter leading to place Pd atoms on top of oxygen sites, according to an epitaxial stacking. This paper shows the results of a basin-hopping global optimization procedure applied to free and MgO-supported Pd clusters in the size range $10 \leq N \leq 120$. Pd−MgO interactions are modeled by an analytical function fitted to ab initio results, while Pd−Pd interactions are modeled by a semiempirical potential. Besides the tight-binding Rosato−Guillopé−Legrand (RGL) potential, we have adopted a modified version of RGL that better reproduces the experimental surface energy of palladium, modifying the attractive part of Pd atoms potential energy. We have compared the two potential models, and as a result, the RGL potential favors clusters with epitaxial arrangements, so that cluster structures are epitaxial fcc in almost all the size ranges considered. On the contrary, the alternative potential model preserves some Ih-like characteristics typical of the free Pd clusters, and it suggests that a transition size from Ih-like to epitaxial structures can take place at about 100 atoms.

I. Introduction

Among nonreactive metal/oxide interfaces, Pd nanoclusters on MgO(100) are a model system for supported catalysts. Palladium on MgO has been widely studied experimentally, because of its efficiency as a catalyst of the CO + NO reaction. Besides measurements of Pd on MgO catalytic activities, experimental and theoretical studies focused on Pd particles size and structures, which are strongly correlated to the characteristics of the catalytic process.

Experimental studies have been primarily interested in the catalytic activity of large Pd particles (from hundreds to several thousands of atoms). From a structural point of view, the observations (by TEM analysis,[1] helium diffraction studies,[2] and grazing incidence small-angle X-ray scattering[3−5]) of Pd clusters on MgO have revealed that Pd clusters show a cube-on-cube epitaxial arrangement on the substrate and the equilibrium shapes for sizes ranging from a few nanometers up to tens of nanometers are squared pyramids and truncated octahedra. Besides experimental works, a theoretical approach proposed by Goniakowski and Mottet[6] has been useful to simulate by molecular dynamics the equilibration of the deposited particles and the substrate-induced characteristics of their morphology. This work has confirmed that the preferred structural ordering of Pd particles is a (100)//(100) epitaxy relation, with some exceptions of a (111)//(100) stabilization. While several direct observations of cluster structures have been performed at these large sizes, the structural characteristics of the smaller clusters can mainly be deduced by their catalytic behavior, roughly similar to the one observed in the Pd(111) flat surface.[7]

In this paper, we address the issue of the most favorable Pd/MgO(100) cluster structure for sizes $10 \leq N \leq 120$ by means of global optimization calculations. The theoretical model we refer to has been presented by Vervisch et al.[8] Pd−Pd interactions are modeled according to a semiempirical tight-binding approach, while the interaction with MgO is described by an analytical function fitted to ab initio calculations.[9] The first focus of this paper is indeed to identify the structural characteristics of free and MgO-supported Pd clusters by means of a basin-hopping global optimization technique. The second focus of the paper is the comparison between two different models of the metal−metal interaction, based on a different weight attributed to the many-body attractive term. We propose a comparison between the results coming from the two models, with the hope to induce further experimental analysis.

The paper is structured as follows: In section II, we describe the model Pd−Pd and Pd−MgO interaction and the global optimization algorithm. The results are collected in section III: structures from free Pd clusters optimizations are shown in section III A, while supported cluster structures are described in III B. Section IV contains a discussion of the results.

II. Model and Method

A. Potential Energy Model. The metal−metal interactions are modeled on the semiempirical many-body potential proposed by Rosato, Guillopé, and Legrand (RGL) in 1989,[10] derived from the electronic structure in the tight-binding second-moment approximation scheme. The potential energy in an N-atom cluster is composed of a many-body bonding term E^b

$$E^b = \sum_{j=1,...N} E_j^b \tag{1}$$

$$E_j^b = -\left[\sum_{i,r_{ji}<r_c} \xi^{1/\alpha} \exp\left[\frac{-q}{\alpha}\left(\frac{r_{ji}}{r_0} - 1\right)\right]\right]^{\alpha} \quad (i = 1, ..., N, i \neq j) \tag{2}$$

and a repulsive Born−Mayer term E^r

* To whom correspondence should be addressed. E-mail: ferrando@fisica.unige.it.
† Dipartimento di Fisica.
‡ Institute of Physical Chemistry "IG Murgulescu".
§ CRMCN-CNRS.

10.1021/jp056599c CCC: $33.50
Published on Web 03/17/2006

$$E^{r} = \sum_{j=1,...N} E_j^{r} \quad (3)$$

$$E_j^{r} = \sum_{i,r_{ji}<r_c} A \exp\left[-p\left(\frac{r_{ji}}{r_0} - 1\right)\right] (i = 1, ..., N, i \neq j) \quad (4)$$

r_{ij} is the distance between the atoms at sites i and j; r_0 is the nearest-neighbors distance in the metallic interaction. Finally, r_c is the cutoff distance for the interaction, here fixed to the value of the third nearest-neighbors distance of bulk palladium. The parameters A, p, q, and ξ are fitted to several bulk experimental values, such as the cohesive energy E_{coh}, the lattice parameter, and the elastic constants B, C_{44}, and C'. In the second-moment approximation adopted by Rosato et al., the attractive part of the potential interaction has a square-root many-body character: the bonding term increases as the square root of the number of first neighbors, Z: $E_j^{b} \propto Z^{0.5}$, that is, $\alpha = 0.5$. In the case of Pd, this model underestimates the surface energy (0.8 J/m^2 instead of 2 J/m^2 for the Pd(100) surface), and the gap between the model and experiment increases with decreasing coordination.[11] To remedy this lack of accuracy, it is possible to modify the dependence of E_j^{b} on Z; this has been performed according to ab initio (FP-LMTO) and tight-binding sp−d hybridized calculations of the densities of states,[12,13] which were compatible with $\alpha = 0.8$.[11] Within this alternative model, the Pd(100) surface energy is 1.5 J/m^2. Parameters referred to both the models are reported in Table 1.

As we will see in detail in the next sections, the $\alpha = 0.5$ potential could agree better with the experimental evidence of epitaxial Pd clusters on the MgO surface. Anyway, we have performed all the global optimizations with both models, to relate the different structural characteristics of global minima to the features of the two potential models and to get an exhaustive comparison between them.

Because of the relatively small electron transfer at the surface, the oxide is expected to produce a quite slight modification of the metal−metal interaction. In our model, the potential energy of each Pd atom is composed of the previous metallic terms plus a free-standing contribution coming from the interaction with MgO. Such metal−oxide interaction requires ab initio calculations to characterize at best the electronic structure and thus the energetics at the interface. In particular, it needs the determination of the adsorption site or the variation of the adsorption energy as a function of metal coverage (1 adatom, 1 monolayer, many layers).[14,15] It is well established that the most favorable adsorption site is located on top of oxygen sites. The adsorption energy is calculated in the framework of the density functional theory (DFT) using the full-potential linearized augmented-plane-wave approach[9] for each type of adsorption site (oxygen, magnesium, and hollow sites) as a function of the elevation above the MgO surface. The potential energy surface (PES) is built via an interpolation between these high-symmetry points. For a Pd atom at site j with coordinates x, y parallel, and z perpendicular to the MgO(100) surface, the metal−MgO(100) interaction is fitted on the ab initio results using the analytical expression

$$E_j^{Pd-MgO}(x, y, z, Z) = a_1(e^{-2a_2(z-a_3)} - 2e^{-a_2(z-a_3)}) \quad (5)$$

with Z being the number of Pd neighbors for atom j. The Z dependence is extrapolated from three different Pd coverages

TABLE 1: Potential Parameters

Pd−Pd interaction	p	q	A	ξ	E_{coh} [eV]
$\alpha = 0.5$	11.00	3.794	0.171	1.702	−3.89
$\alpha = 0.8$	8.13	5.02	0.524	1.370	−3.89

(adatom, $Z = 0$; monolayer, $Z = 4$; bilayer, $Z = 8$) with the following expressions

$$a_i(x, y, Z) = b_{i1} + b_{i2}e^{-Z/b_{i3}} \quad (6)$$

Finally, the (x, y) dependence is given by

$$b_{ik}(x, y) = c_{ik1} + c_{ik2}\left[\cos\left(\frac{2\pi}{l}x\right) + \cos\left(\frac{2\pi}{l}y\right)\right] + c_{ik3}\left[\cos\left(\frac{2\pi}{l}(x+y)\right) + \cos\left(\frac{2\pi}{l}(x-y)\right)\right] \quad (7)$$

where l is the lattice parameter of MgO. The 27 parameters of the Pd−MgO interaction are listed at the web page http://www.crmcn.univ-mrs.fr/gModel/webparam.pdf.

B. Global Optimization Algorithm. For a general reference to basin hopping, see ref 16. We have performed the global optimization of Pd clusters on MgO in the size range $10 \leq N \leq 120$, using both the $\alpha = 0.8$ and the $\alpha = 0.5$ interaction models. The basin-hopping algorithm we have used presents a very simple implementation: starting from a random local minimum, the supported Pd cluster is iteratively modified. Moves consist of displacing every atom inside a sphere centered in its current position, to obtain a shaking of the present configuration; the sphere radius has been kept fixed at 1.3 Å. After this, the cluster is locally minimized and the new configuration is compared to the current one. The current configuration is updated according to a Metropolis algorithm

$$p_{accept} = \min\{1, \exp[-(E_{final} - E_{initial})/(k_B T)]\} \quad (8)$$

The whole move is thus accepted with probability $p_{accept} = 1$ if the final energy is lower than the initial one, while if the final energy is higher, the move is accepted with the standard Boltzmann probability factor.

Two different kinds of local minimizations are possibile within our algorithm: (1) a quenching procedure based upon a molecular dynamics (MD) scheme[17] and (2) the use of the limited memory algorithm for bound constrained optimization called *lbfgsb*.[18] Starting from a random configuration of Pd atoms, the program has been allowed to evolve through a size-dependent number of Monte Carlo steps ($n_{MC} \simeq 20\,000$ for the smallest clusters and $n_{MC} \simeq 120\,000$ for the largest). For each size, we have performed at least five independent optimization runs, with the temperature parameter fixed at $T = 2500$ K. We have chosen this temperature, which is somewhat higher than the melting temperature of bulk Pd, to get an efficient sampling of the PES.

III. Results

A. Free Pd Clusters: Minima Obtained with $\alpha = 0.5$ and $\alpha = 0.8$. Looking at the surface energies of the (111) and (100) facets corresponding to the two different models,[11] we can observe that, beyond the good agreement of the $\alpha = 0.8$ model to the experimental data, in the $\alpha = 0.8$ case, the difference between σ_{100} and σ_{111} is enlarged with respect to the $\alpha = 0.5$ case. As we will see through the analysis of the minima located by the two model potentials, these different energy gaps correspond to a preference of the $\alpha = 0.8$ potential for structures exposing large (111) facets, like icosahedral (Ih) structures, so

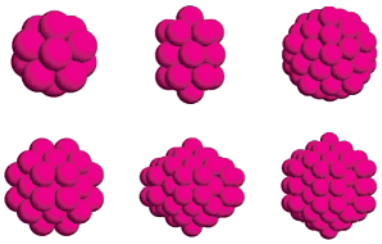

Figure 1. Magic cluster structures in the size range considered. According to RGL potential, these structural arrangments are the global minimum configurations for the most part of noble and transition metals.[21]

disfavoring (100) facets typical of face centered cubic (fcc) and decahedral (Dh) ordering. This indication is confirmed by the results of the global optimization of pure Pd clusters. Previous calculations based on a RGL model ($\alpha = 0.5$)[19] have shown that the structural transition from Ih-like to Dh-like minima is located below 100 atoms size, and the Dh range is extended up to several thousands of atoms. According to calculations by Goniakowski et al.,[11] applied to magic size clusters, with the $\alpha = 0.8$ model, the transition size from Ih to Dh ordering is increased up to 1000 atoms, and the next Dh to fcc transition moves from 10 000 to 20 000 atoms. In the size range here considered, we can find several magic sizes for different geometrical arrangements: $N = 13$ and 55 are magic sizes for icosahedra, $N = 19$ corresponds to a small polyicosahedron (pIh), $N = 38$ is the magic size for the fcc truncated octahedron (TO), and $N = 75$ and 101 correspond to complete decahedral structures (see Figure 1). In the following, we will see that both the models considered ($\alpha = 0.8$, $\alpha = 0.5$) preserve the magic structures of the global minimum configurations at the magic sizes but enlarge or narrow the stability ranges of the different geometrical arrangments.

Figure 2 shows the parameters Δ and Δ_2 vs cluster size, for both the potential models. As usual,[20] in an N-atom cluster, Δ is defined as the difference between the total potential energy and the bulk cohesive energy of N atoms

$$\Delta = \frac{E_N - N\epsilon^{\mathrm{coh}}}{N^{2/3}} \tag{9}$$

The number of surface atoms scales roughly as $N^{2/3}$, so that the denominator is useful to compare clusters of different sizes. The smaller the Δ value, the better the energetic configuration. Δ_2 is defined as

$$\Delta_2 = -2E_N + E_{N-1} + E_{N+1} \tag{10}$$

Maxima of the values of Δ_2 correspond to global minimum structures that present a stable energetic configuration with respect to those of the nearby sizes.

Figure 2 refers to the sub-interval $40 \leq N \leq 80$, because in this size range several differences between the two models can be pointed out. We start analyzing the minima corresponding to the $\alpha = 0.5$ model, which present a large predominance for Dh and fcc structures. Only 4 Ih global minima have been located (and no more icosahedra have been found up to $N = 120$). According to both Δ and Δ_2 analysis, a stable decahedral minimum can be found at $N = 43$, and at size $N = 48$, the global minimum is a decahedron covered by hcp islands (see Figure 3). Unlike the prediction of the RGL potential for other transition metals (Ag, Cu, Au, Pt, Ni, see ref 21), Δ and Δ_2 reveal that the magic size for the icosahedral arrangement is located at size $N = 54$ and not $N = 55$. The best structure at $N = 54$ has indeed an icosahedral symmetry but misses its central atom (see again Figure 3 and ref 22). Except for $N = 46$, the only Ih minima that have been located are placed around the $N = 54$ minimum: the $N = 53$ cluster is the 54 Ih missing a surface vertex, while the complete icosahedron is the global minimum at size 55. The size $N = 56$ can thus be defined as the starting point of a large decahedral range: according to the $\alpha = 0.5$ parametrization, Dh begin to be strongly favored far below 100 atoms. High-symmetry Dh configurations with low Δ and high Δ_2 values can be found at $N = 64$ and $N = 71$, and at $N = 75$, the global minimum cluster is the (2,2,2) Marks decahedron. Several global minima exhibit an fcc geometrical arrangement. Below $N = 40$ atoms, the best Δ value corresponds to the perfect TO encountered at $N = 38$, while the next fcc structure with a high stability has been located at $N = 79$ (another TO structure, see Figure 4).

Our calculations based on the $\alpha = 0.5$ model are in good agreement with the global minimum structures obtained by Massen et al.[23] in the size range $10 \leq N \leq 55$ (they used the same kind of potential, with a different parametrization).

Looking at the sequence of $\alpha = 0.8$ minima, one first notices that it is characterized by a large Ih range centered in the perfect 55-atom icosahedron, followed by a sequence of decahedral structures. One can note that beyond $N = 100$ the transition to the Dh range is not yet achieved because Ih_{147}-based minima have been found. The fcc structures are nearly absent: the only fcc minima in the $5 \leq N \leq 120$ range are located at $N = 38$ (TO) and $N = 80$. Moreover, while in the $\alpha = 0.5$ sequence, the TO structure is the global minimum configuration at size $N = 39$ and 40 as well (TO plus 1 and 2 atoms placed on top of (100) facets); the $N = 39$ and 40 cluster structure in the $\alpha = 0.8$ sequence is a decahedron. Good minima according to Δ and Δ_2 values can be pointed at $N = 46$, 48, and obviously 55 (all with an icosahedral arrangement) and $N = 67$, 71, and 75 (decahedral, see Figures 3 and 4).

To gain insight into the different tendency of the two potential models to favor the presence of (100) facets on the cluster surface, we can consider the global minimum cluster at size $N = 71$ (see Figure 4). According to both models, the best cluster is a fragment of the (2,2,2) Marks decahedron, and in both cases, Δ and Δ_2 values point to it as a stable cluster. This cluster exhibits a squared (100) 3×3 facet on its surface (by covering the four fcc sites of this facet, one would obtain the perfect (2,2,2) Marks Dh). Table 2 shows the values of the total potential energy of the $N = 71$ cluster and of the (100) facet both according to $\alpha = 0.8$ and $\alpha = 0.5$. The atom at the center of the (100) facet is less compressed in the case of $\alpha = 0.5$, so that the (100) facet is slightly better accommodated by the $\alpha = 0.5$ cluster.

As we are going to show in the following, the different behavior of the two metallic bonding in favoring fcc structures and (100) facets is of fundamental importance in determining the characteristics of the supported Pd clusters.

B. MgO-supported Pd Clusters: Minima Obtained with $\alpha = 0.5$ and $\alpha = 0.8$. The free clusters analysis has shown that the two models for the metallic interactions have a different tendency to favor Ih, Dh, and fcc structures. What happens when the metallic potentials are coupled to the substrate interaction? On one hand, experimental evidence would suggest that the interaction with the substrate is able to force an fcc and epitaxial ordering for Pd clusters on the MgO(100) surface. On the other hand, small free clusters seldom adopt a bulk arrangment, because this disfavors the energetic configuration of the cluster surface. For supported Pd clusters, the equilibrium structure of

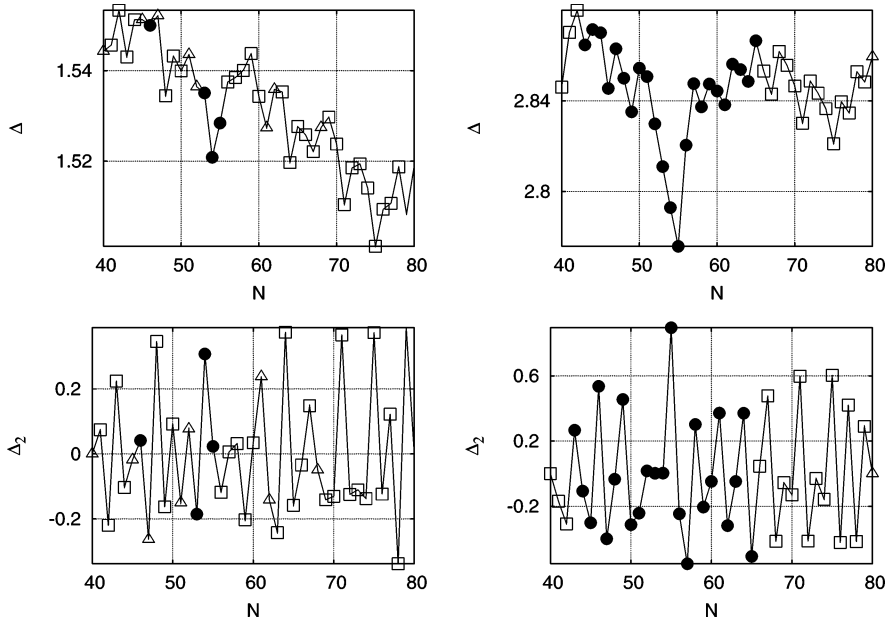

Figure 2. Δ and Δ_2 values referred to the $40 \leq N \leq 80$ size range of the two sequences of the global minimum structures for free Pd clusters. The left column refers to the $\alpha = 0.5$ results, the right one to the $\alpha = 0.8$ results. Full circles indicate that the cluster structure is Ih-like, squares indicate Dh-like clusters, and triangles refer to fcc arrangments.

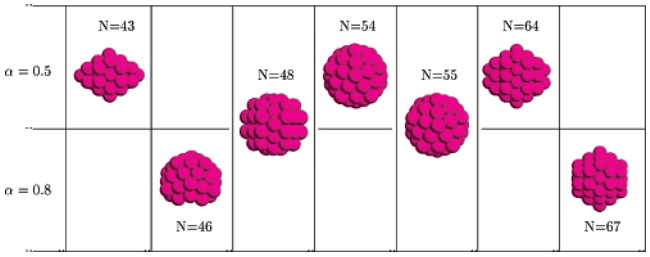

Figure 3. Snapshots of the $\alpha = 0.5$ and $\alpha = 0.8$ structures characterized by the best Δ and Δ_2 values. On the top row ($\alpha = 0.5$), the hollow $N = 54$ Ih appears in the narrow range of the icosahedral minima, surrounded by a large decahedral range. Even if the Dh at $N = 48$ is the global minimum for both parametrizations, in the case of $\alpha = 0.8$, the icosahedral range is larger, extending from $N = 43$ up to $N = 64$.

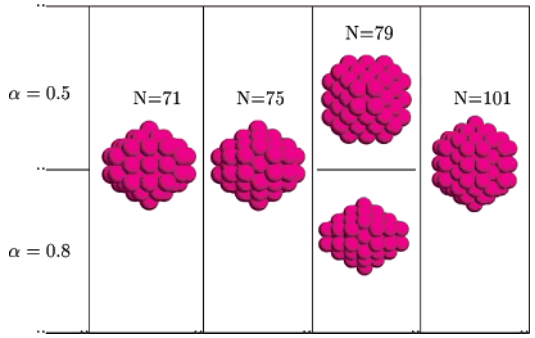

Figure 4. Decahedral minima are common to both the parametrizations at sizes $N = 71$, 75, and 101. At size $N = 79$, the $\alpha = 0.5$ potential exhibits an fcc global minimum.

TABLE 2: $N = 71$ Cluster Energy

Pd−Pd interaction	E_{71} [eV]	$E_{71}^{(100)}$ [eV]	%
$\alpha = 0.5$	−250.292	−30.504	12.2
$\alpha = 0.8$	−227.663	−26.643	11.7

the cluster derives from the competition between a good adhesion to the oxide surface (which favors fcc and epitaxial ordering, exposing large (100) facets parallel to the MgO layer) and a configuration respectful of the metallic bond order−bond length correlation.[24] Experimentally, the small epitaxial Pd cluster on MgO, as first observed by Giorgio et al.,[25] has a first layer with ≃2 nm diameter, so being beyond the upper limit of the clusters analyzed here (for $N = 120$, the diameter is ≃1.5 nm). Our aim here is to propose, in the framework of the comparison between the two potential models adopted, a description of the structural transition of supported clusters from the Ih and Dh range to the fcc epitaxial one.

To quantify the stability of the supported minima, we need a modified definition of the Δ parameter. Our choice consists of regarding separately the interaction with the substrate and the stability of the metallic arrangement; to express how much the geometrical ordering is favorable from the point of view of the metal−metal interaction, Δ parameter is redefined as

$$\Delta = \frac{E_N - E_N^{\mathrm{Pd-MgO}} - N\epsilon^{\mathrm{coh}}}{N^{2/3}} \tag{11}$$

where $E_N^{\mathrm{Pd-MgO}}$ is the energy of interaction with the substrate. We take into account the Pd−substrate bonds of an N-atom cluster simply considering the interaction energy $E_N^{\mathrm{Pd-MgO}}$. In regards to Δ_2, its definition does not change.

Our analysis starts with the results coming from the $\alpha = 0.5$ model. The sequence of global minima is characterized by the immediate (from $N = 11$ on) transition from 5-fold symmetry based structures to fcc epitaxial structures. According to this model, the substrate is able to force an epitaxial arrangement and disfavor Ih- and Dh-like structures. Leroy et al.[4] have shown by in situ X-ray scattering experiments that, if the growth temperature is high enough to let the clusters adopt their equilibrium shape ($T = 650$ K and above), it can be observed that different sizes correspond to different epitaxial arrangements: from small pyramidal particles to larger truncated octahedra. Within the latter geometrical family, pyramids are truncated both on the top and in the layer in contact with the substrate. Moreover, molecular dynamics simulations based on the RGL second-moment approximation model[6] have predicted the presence of a missing-edge Pd layer at the oxide interface of Pd clusters.

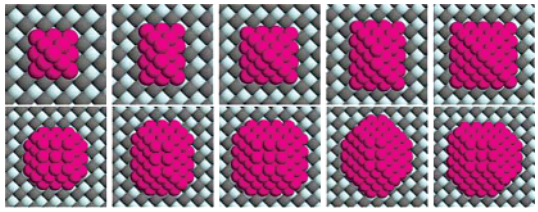

Figure 5. Some snapshots from the sequence of supported minima obtained with the $\alpha = 0.5$ parametrization. In the top row, the global minima with a perfect pyramidal structure ($N = 14$, 20, 30, 40, and 55). In the bottom row, some of the truncated pyramids that occur more and more frequently with increasing cluster size ($N = 46$, 64, 82, 94, and 113). Substrate light and dark atoms represent, respectively, oxygen and magnesium atoms.

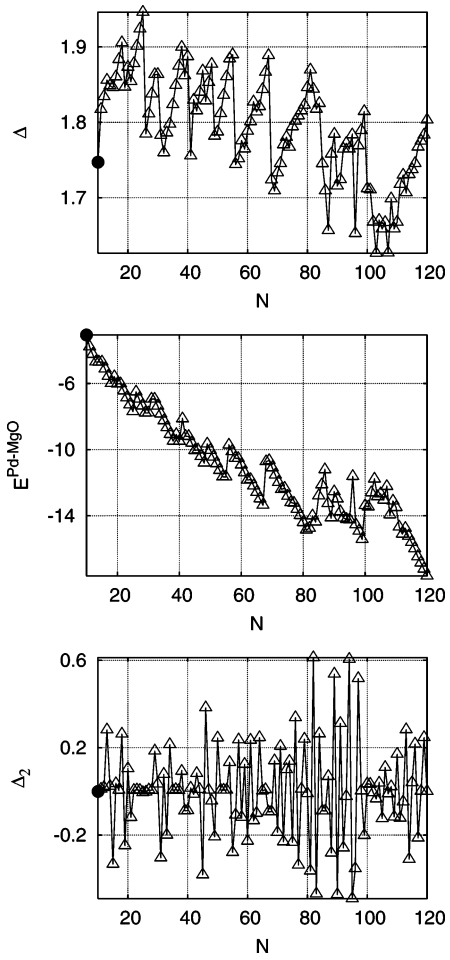

Figure 6. Δ, $E^{\mathrm{Pd-MgO}}$, and Δ_2 for supported clusters as a function of size N. Panels refer to $\alpha = 0.5$ parametrization. From the top, the two indicators of the stability for metallic bonding and Pd−MgO interaction, respectively, Δ and $E^{\mathrm{Pd-MgO}}$, are shown. In the bottom row, Δ_2 values are reported. The full circle refers to an Ih-like structure, triangles to fcc epitaxial structures.

In the size range $11 \leq N \leq 65$ (see the top row of Figure 5), all structures are of the pyramid type. These clusters show a complete or missing-edge layer in contact with MgO. Perfect pyramidal shapes can be found at $N = 14$ (3×3 atoms in the first layer), $N = 20$ (3×4), $N = 30$ (4×4), $N = 40$ (5×4), and $N = 55$ (5×5). Looking at Figure 6, one can observe that pyramidal magic sizes correspond to good values of the interaction with MgO(100) but also to bad Δ values. This can be explained by the presence of low-coordination atoms both on top of pyramids and on their bottom layer. We find pyramids missing one or more corner atoms (as $N = 34$ and 46) and also clusters which miss at least one whole edge of their bottom layer. The latter are more likely to be found with increasing size (see Figure 5). All of these incomplete pyramids have low Δ_2 values. Among them, $N = 46$, 82, and 94 have good stability both from the point of view of the comparison with their nearby sizes and from the point of view of their interaction with the substrate.

To highlight the differences between the pyramidal and the truncated structures, we can consider the example of the clusters located at sizes $N = 82$ and $N = 91$. The global minimum cluster for $N = 82$ is a squared pyramid (6×6) truncated on the top (missing five atoms of its top two layers) and at the vertexes of its first layer (missing four atoms). As expected, the perfect pyramidal structure of size $N = 91$ that can be built up by adding the nine missing atoms is not favorable: even if the large 6×6 squared base ensures a higher adhesion to the substrate ($E_{\mathrm{adh}} = -16.3104$ eV) than in the global minimum (GM) structure ($E_{\mathrm{adh}} = -14.1208$ eV), the GM structure has a lower energy overall: $E_{91,\mathrm{GM}} = -332.0892$ vs $E_{91,\mathrm{pyramidal}} = -331.5464$.

Truncated pyramids and missing-edge pyramids become more and more favorable as the cluster size increases: the next peak among the Δ_2 values is $N = 94$. This global minimum results from the truncation of the perfect 6×7 pyramid (see Figure 5). The square-base motif is again present around size $N = 113$: in this case, the truncation involves, respectively, three and two complete rows of atoms of the first layer, so generating a re-entrant morphology.

Let us move to the sequence of minima obtained with $\alpha = 0.8$. Unlike the $\alpha = 0.5$ case, up to $N = 50$, the substrate influence is not strong enough to force a stable fcc structural arrangment of Pd clusters. As we have previously noted, a large icosahedral range characterizes the free cluster sequence. As a result of the supported $\alpha = 0.8$ cluster minimizations, the interaction with MgO is strong enough to reduce the Ih range but not to suppress it. To sum up, within the $\alpha = 0.8$ model, the algorithm has located three kinds of structures: (a) Ih-based clusters at the small sizes and several Dh-based minima at medium sizes, (b) fcc clusters with (111) facets parallel to the substrate (medium size), and (c) fcc clusters with (100) facets parallel to the substrate and hcp islands on their surface (large size). With regards to (a) minima, fragments of the free $N = 55$ atoms Ih, with a good Δ value, are the supported global minimum structures at sizes $N = 45$, 46, 47, 48, and 49 (see Figures 7 and 8). On one hand, the icosahedral structures have low Δ values ($N = 49$ has the best metallic configuration of the whole sequence, as can be seen in Figure 7), but on the other hand, all of these Ih-based structures do not match the substrate pattern as well as the fcc structures do and they exhibit a poor Pd−MgO interaction energy (see again Figure 7).

As size increases from $N = 50$, some Dh-based structures (see Figure 8) have also been located in this sequence. The low Δ configuration at $N = 89$, for example, is a fragment of a decahedron exposing a 3×4 rectangular (100) facet on the bottom, matching the substrate. Pd−MgO interaction energy is not as good as the one of the fcc nearby minima, because the number of atoms laying in contact with MgO is lower than at $N = 85$, 86, 87, 88, and 90. Another Dh-based structure is the global minimum energy configuration at $N = 77$.

Structures (b) and (c) reveal that also for $\alpha = 0.8$ the influence of the substrate becomes more and more strong with increasing cluster radius. The presence of the (111) or (100) facet, parallel to the substrate, on the cluster surface corresponds, respectively, to a bad or good match to the MgO pattern. As an example, Figure 9 shows the layer in contact with MgO for the minimum clusters of size $N = 111$ (fcc, epitaxial with an hcp island on

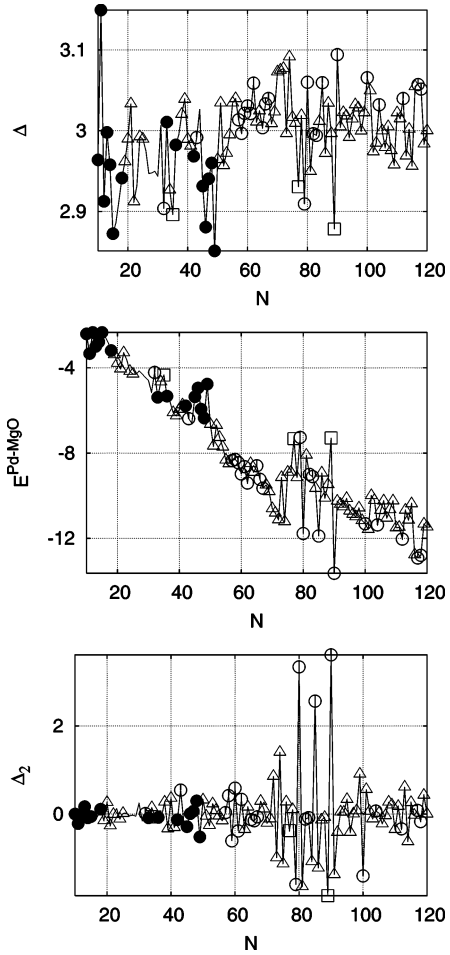

Figure 7. Δ, E^{Pd-MgO}, and Δ_2 for supported clusters as a function of size N. Panels refer to $\alpha = 0.8$ parametrization. From the top, the two indicators of the stability for metallic bonding and Pd−MgO interaction, respectively, Δ and E^{Pd-MgO}, are shown. In the bottom row, Δ_2 values are reported. Full circles refer to Ih-like structures, squares to Dh-like, blank circles to (111)-base fcc structures, and triangles to fcc epitaxial structures.

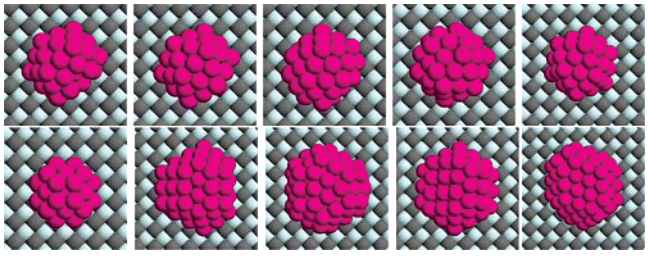

Figure 8. Some snapshots of the global minima located in the series of supported clusters, $\alpha = 0.8$. In the first row, the structures based on fragments of the free $N = 55$ Ih structure ($N = 45$, 46, 47, 48, and 49). In the bottom row, the first picture is the smallest epitaxial cluster found in the whole sequence, $N = 34$, based on the perfect truncated octahedron, that is, the free clusters global minimum at $N = 38$; in the second and fourth positions, there are two decahedral clusters, $N = 77$ and 89. $N = 89$ is covered by islands in stacking fault positions. The third and the last clusters of the bottom row are fcc but not epitaxial minima, $N = 79$ and $N = 90$. These clusters have (111) facets in contact with the substrate.

its surface) and $N = 112$ (fcc but not epitaxial). As a general trend, the mismatch between the (111) facets ordering and the substrate, which should not favor the quality of the Pd−MgO interaction, is partially compensated by a higher number of atoms in contact with it. As observed in the previous sections, the $\alpha = 0.8$ parametrization strongly penalizes low-coordinated

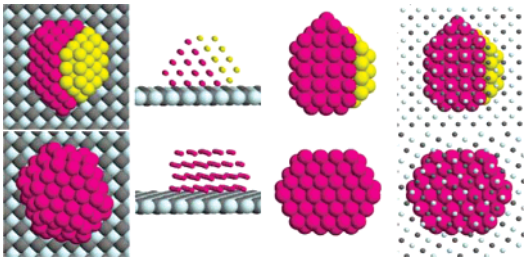

Figure 9. In the sequence of $\alpha = 0.8$ supported clusters, the global optimization procedure has located both fcc, epitaxial clusters, and fcc, not epitaxial clusters. The top row shows the minimum located at $N = 111$. This is a fcc epitaxial cluster with hcp islands on its surface (light palladium atoms). The third and fourth snapshots of the row show the bottom layer of the cluster and its matching with the MgO substrate: a (100) facet composed of 22 atoms leans on the surface. In the bottom row, the $N = 112$ atom cluster is shown. Unlike $N = 111$, this cluster does not match the substrate lattice and has a (111) facet parallel to the oxide surface. In this latter case, the first layer of the clusters contains 32 atoms, and because of this large number of atoms in contact with the surface, the Pd−MgO interaction energy is comparable to that of epitaxial structures.

atoms of the (100) facets, so forcing a strong competition between (b) and (c) clusters even at larger sizes.

IV. Conclusions

In this paper, we have shown the results of the global optimization of Pd clusters on an MgO surface, in the size range $10 \leq N \leq 120$. Global optimization has been performed by means of a basin-hopping algorithm.

For each cluster size, we have located the two putative global minimum cluster structures corresponding to two different model potentials. Both the potentials have many-body character in their attractive term, but while the RGLs attractive part presents a dependence on $Z^{0.5}$, the alternative potential proposed by ref 11 modifies it, introducing a $Z^{0.8}$ dependence that ensures a better fit of the potential to the experimental values of Pd surface energies.

To get a first insight in the kind of structures favored by the two different potentials, we performed the optimization of free Pd clusters in the sequence of clusters with size $N = 10$, 11, ..., 120. The $\alpha = 0.5$ model disfavors icosahedral arrangements, because it presents a stronger bond order−bond length correlation than the $\alpha = 0.8$ model, the latter being more similar to the linear Z dependence. As a result, we have highlighted the strong prevalence of decahedral structures for the $\alpha = 0.5$ potential, with a larger influence of the icosahedral motif in the sequence of global minima coming from the $\alpha = 0.8$ potential.

This difference becomes even more important when Pd clusters are in contact with the (100) surface of MgO, and the interaction with the substrate has an increasing influence on clusters structures with enlarging cluster size . The sequence of supported global minima with $\alpha = 0.5$ is indeed characterized by the stronger MgO influence: minima exhibit an fcc ordering, often epitaxial with respect to the (100) surface. As suggested by previous experiments on MgO-supported Pd clusters, pyramidal structures and truncated-octahedral clusters are the most common structural motifs of the sequence. On the contrary, the small sized minima obtained with the $\alpha = 0.8$ potential often preserve their icosahedral character, and transition from Ih-like structures to fcc epitaxial structures goes through an intermediate range of clusters exposing a large (111) facet on the MgO substrate. The epitaxial arrangement becomes more and more

frequent as size increases, but some clusters with a (111) base have been located for $N \geq 100$ as well.

To sum up, according to our $\alpha = 0.5$ results, the transition from Ih-like structures to fcc epitaxial structures seems to take place just above 10 atoms, but according to the $\alpha = 0.8$ model, this is not the case and up to $N = 120$ atoms the transition to the experimentally observed epitaxial clusters is not yet completed, pushed upward by the presence of the (111) base clusters. The smallest fcc and epitaxial Pd/MgO(100) cluster ever observed[25] is about 1 nm large, but it is not possible to assign it a precise size. Previous experiments by Wörz[7] regarding very small MgO-supported Pd clusters have revealed that, in the size range $N \leq 30$, the Pd clusters act as very good catalysts of the CO + NO reaction. The catalytic process, in this narrow size range, can take place at very low temperature, up to 300 K lower than using Pd particles with radius larger than 2 nm. The activation of different reaction patterns on the surface of these small clusters suggests that, in the size range considered in this paper, a structural transition should be located. These experimental results seem to be in better agreement with the outcome of the $\alpha = 0.5$ model.

The comparison between the two models thus appears as a useful tool to understand the nature of the Pd−Pd interaction on the MgO(100) surface, and the results presented here can suggest a further experimental investigation.

Acknowledgment. The authors thank Claude Henry for fruitful discussions. They also acknowledge financial support from the Italian CNR for the project SSA-TMN within the framework of the ESF EUROCORES SONS and from the European Commission for the project GSOMEN (Contract No. NMP4-CT-2004-001594).

References and Notes

(1) Graoui, H.; Giorgio, S.; Henry, C. R. *Surf. Sci.* **1998**, *417*, 350.
(2) Henry, C. R.; Meunier, M. *Mater. Sci. Eng., A* **1996**, *217/218*, 239.
(3) Renaud, G.; et al. *Science* **2003**, *300*, 1416.
(4) Leroy, F.; Revenant, C.; Renaud, G.; Lazzari, R. *Appl. Surf. Sci.* **2004**, *238*, 233.
(5) Revenant, C.; Leroy, F.; Lazzari, R.; Renaud, G.; Henry, C. *Phys. Rev. B* **2004**, *69*, 035411.
(6) Goniakowski, J.; Mottet, C. *J. Cryst. Growth* **2005**, *275*, 29.
(7) Wörz, A. S.; Judai, K.; Abbet, S.; Heiz, U. *J. Am. Chem. Soc.* **2003**, *125*, 7964.
(8) Vervisch, W.; Mottet, C.; Goniakowski, J. *Phys. Rev. B* **2002**, *65*, 245411.
(9) Giordano, L.; Goniakowski, J.; Pacchioni, G. *Phys. Rev. B* **2001**, *64*, 075417.
(10) Rosato, V.; Guillopé, M.; Legrand, B. *Philos. Mag. A* **1989**, *59*, 321.
(11) Goniakowski, J.; Mottet, C.; Noguera, C. Scientific highlight of the month. *Psi-k Newsletter*, 2004, Vol. 62, p 85.
(12) Sawaya, S.; Goniakowski, J.; Mottet, C.; Saul, A.; Trèglia, G. *Phys. Rev. B* **1997**, *56*, 12161.
(13) Mottet, C.; Trèglia, G.; Legrand, B. *Surf. Sci.* **1996**, *352*−*354*, 675.
(14) Goniakowski, J. *Phys. Rev. B* **1998**, *57*, 1935.
(15) Goniakowski, J. *Phys. Rev. B* **1998**, *58*, 1189.
(16) Doye, J. P. K.; Wales, D. J. *J. Phys. Chem. A* **1997**, *101*, 5111.
(17) Bennett, C. H. *Diffusion in Solids, Recent Developments*; Norwick, A. S., Burton, J. J., Eds.; Academic: New York, 1975.
(18) Byrd, R. H.; Lu, P.; Nocedal, J.; Zhu, C. Technical Report NAM-08; University of Colorado: Boulder, CO, 1994.
(19) Baletto, F.; Ferrando, R.; Fortunelli, A.; Montalenti, F.; Mottet, C. *J. Chem. Phys.* **2002**, *116*, 3856.
(20) Rossi, G.; Ferrando, R.; Rapallo, A.; Fortunelli, A.; Curley, B. C.; Lloyd, L. D.; Johnston, R. L. *J. Chem. Phys.* **2005**, *122*, 194309.
(21) Baletto, F.; Ferrando, R. *Rev. Mod. Phys.* **2005**, *77*, 371.
(22) Mottet, C.; Goniakowski, J.; Baletto, F.; Ferrando, R.; Tréglia, G. *Phase Transitions* **2004**, *77*, 101.
(23) Massen, C.; Mortimer-Jones, T. V.; Johnston, R. L. *J. Chem. Soc., Dalton Trans.* **2002**, 4375.
(24) Pauling, L. *The Nature of Chemical Bond*; Cornell University Press: New York, 1960.
(25) Giorgio, S.; Chapon, C.; Henry, C. R. *Philos. Mag. B* **1993**, *67*, 773.